

# A QUANTUM KINETIC MONTE CARLO METHOD FOR QUANTUM MANY-BODY SPIN DYNAMICS\*

ZHENNING CAI<sup>†</sup> AND JIANFENG LU<sup>‡</sup>

**Abstract.** We propose a general framework of quantum kinetic Monte Carlo algorithm, based on a stochastic representation of a series expansion of the quantum evolution. Two approaches have been developed in the context of quantum many-body spin dynamics, using different decomposition of the Hamiltonian. The effectiveness of the methods is tested for many-body spin systems up to 40 spins.

**Key words.** Spin dynamics, quantum kinetic Monte Carlo, Dyson series

**AMS subject classifications.** 74S60

**1. Introduction.** We consider the system with  $N$  spins in a magnetic field, which is given by the Hamiltonian

$$(1.1) \quad H(t) = \sum_{k=1}^N m^{(k)}(t) \cdot \sigma^{(k)} + \sum_{1 \leq j < k \leq N} \gamma_{jk}(t) \sigma^{(j)} \cdot \sigma^{(k)}$$

with Hilbert space of the quantum system given by  $\mathcal{H} = (\mathbb{C}^2)^{\otimes N}$ . For every  $k = 1, \dots, N$ , the operator  $\sigma^{(k)}$  denotes the Pauli matrices acting on the  $k$ -th spin:

$$(1.2) \quad \sigma^{(k)} = (\sigma_1^{(k)}, \sigma_2^{(k)}, \sigma_3^{(k)})^\top, \quad \sigma_i^{(k)} = \text{Id}^{\otimes(k-1)} \otimes \sigma_i \otimes \text{Id}^{\otimes(N-k)};$$

where  $\text{Id}$  stands for the identity operator acting on a single spin ( $\mathbb{C}^2$ ). The first term on the right hand side of (1.1) gives the single-body Hamiltonians, where  $m^{(k)}(t) = (m_1^{(k)}(t), m_2^{(k)}(t), m_3^{(k)}(t))^\top$  is the magnetic field acting on the  $k$ th spin. For the two-body interaction in the Hamiltonian (1.1), we have used the notations

$$(1.3) \quad \sigma^{(j)} \cdot \sigma^{(k)} = \sigma_1^{(j)} \sigma_1^{(k)} + \sigma_2^{(j)} \sigma_2^{(k)} + \sigma_3^{(j)} \sigma_3^{(k)},$$

$$(1.4) \quad \sigma_i^{(j)} \sigma_i^{(k)} = \text{Id}^{\otimes(j-1)} \otimes \sigma_i \otimes \text{Id}^{\otimes(k-j-1)} \otimes \sigma_i \otimes \text{Id}^{\otimes(N-k)}.$$

Thus  $\sigma^{(j)} \cdot \sigma^{(k)}$  counts for a Heisenberg type interaction between the  $j$ -th and  $k$ -th spins with  $\gamma_{jk}(t)$  being the interaction strength or coupling intensity.

This paper concerns numerical algorithm for the time evolution of the system: The many-body wave function  $|\Psi\rangle \in \mathcal{H}$  is govern by the Schrödinger equation

$$(1.5) \quad \frac{d}{dt} |\Psi\rangle = -iH |\Psi\rangle.$$

While (1.5) is a linear ODE system, solving the system directly is impractical even for dozens of spins, as the size of the system  $\dim \mathcal{H} = 2^N$  grows exponentially as

\*This work is partially supported by the National Science Foundation under Grant Nos. DMS-1454939 and RNMS11-07444 (KI-Net). Zhenning Cai is also supported by National University of Singapore Startup Fund under Grant No. R-146-000-241-133. The authors would like to thank Gero Friesecke for suggesting the problem and for illuminating discussions.

<sup>†</sup>Department of Mathematics, National University of Singapore, Level 4, Block S17, 10 Lower Kent Ridge Road, Singapore 119076 ([matcz@nus.edu.sg](mailto:matcz@nus.edu.sg)).

<sup>‡</sup>Department of Mathematics, Department of Physics, Department of Chemistry, Duke University, Box 90320, Durham NC 27708, USA ([jianfeng@math.duke.edu](mailto:jianfeng@math.duke.edu)).

the number of spins increases. In fact, even representing a particular state  $|\Psi\rangle$  is challenging: for  $N = 40$ , the size of the vector is greater than 1 trillion; not mentioning the computational cost involved in evaluation the matrix-vector product  $H|\Psi\rangle$ .

While the Hamiltonian (1.1) is rather general, our algorithm development is mainly motivated by applications in nuclear magnetic resonance (NMR) [3], where the nuclear spins react to magnetic fields. In such applications, for the coefficient of the single body term  $m(t) = (m_1(t), m_2(t), m_3^{(k)})^\top$ ,  $(m_1(t), m_2(t))$  is prescribed as a control field (such that the control magnetic field is only in  $(x, y)$  direction) and the time independent  $m_3^{(k)}$  is understood as an energy splitting of the  $|\uparrow\rangle$  and  $|\downarrow\rangle$  states of the  $k$ -th spin. The  $\gamma_{jk}$  terms account for dipole-dipole interactions between the nuclear spins, and the magnitude of which decays very fast as the distance between nuclei increases and is usually quite small compared to the energy splitting and the external fields. The value of these coefficients might contain some uncertainty due to experimental imperfectness. One potential application of our method is robust control of NMR via pulse design (see e.g., [4] and references therein) when the spin-spin interactions are taken into account, which we will leave for future works.

The high dimensionality of the system naturally calls for Monte Carlo type methods. The motivation of the algorithm proposed in this work comes from a surface hopping method recently developed by us in [1], which can be viewed as a stochastic method to solve generic high dimensional ODE systems (or PDE systems combined with some particle / semiclassical methods, as in [9, 1]). The overall idea of the algorithm contains two elements:

1. a series expansion of the solution of the system based on a time-dependent perturbation theory, *i.e.*, from the ODE point of view, a repeated back-substitution in the integral form of the system based on Duhamel’s principle;
2. a Monte Carlo method to stochastically evaluate the series expansion based on an efficient representation of part of the Hilbert space.

In this work, we will apply the above framework to develop methods for quantum many-body spin dynamics. For a particular system, to make the algorithm efficient, it is crucial to identify a suitable “small term” to be used in the series expansion from time-dependent perturbation theory. In the setting of spin dynamics, we will discuss two approaches: 1) one is based on a decomposition of the Hamiltonian into terms commuting with  $\sigma_3$  and those not commuting (*i.e.*, diagonal and off-diagonal terms in the  $Z$ -basis of the spins); 2) the other approach is based on a splitting of the Hamiltonian into single-body term and two-body interactions.

Over the years, many numerical methods have been developed in physics and chemistry literature for many-body quantum dynamics, which is a central challenge in theoretical understanding of quantum systems. While a complete literature review is beyond the scope, we discuss here some related works to our approach.

The methods proposed in the literature can be roughly categorized into two groups. One class of methods is based on an efficient representation of the relevant part of the Hilbert space of the many-body quantum system, such as the multi-configurational time-dependent Hartree (MCTDH) [10], originally developed for the nucleus dynamics, which uses multi-configurational Hartree ansatz to represent wave functions. Other methods belong to this class include the time-evolving block decimation (TEBD) [17] and the time-dependent density matrix renormalization group (tDMRG) [15] as extensions of the DMRG method [18] to dynamical problems. These methods are based on matrix product states and hence rather powerful for one (physical) dimensional systems, but face difficulty in extending to higher dimensions.

The other class of methods is based on Monte Carlo sampling. A particular relevant class of quantum Monte Carlo methods to our method is the continuous-time quantum Monte Carlo (CT-QMC) [13, 12, 5], which can be understood as a continuum time limit of the Trotter splitting based Hirsch-Fye QMC method [6]. While the CT-QMC method was originally developed for imaginary time propagation, it has also been extended to real time dynamics in recent years [11, 2], in particular for impurity models in condensed matter physics. Another related quantum Monte Carlo method is the auxiliary field quantum Monte Carlo [20, 19] based on the Hubbard-Stratonovich transformation [7, 16], which represents the imaginary time evolution of the many-body electronic wave function as a stochastic sum of Slater determinants. We also note a different strategy – discrete truncated Wigner approximation (DTWA) – proposed recently [14] based on a tensor product ansatz on the level of discrete Wigner representation of many-body spin density matrix. The Monte Carlo method is used to sample initial states according to the phase space distribution.

Our method can be understood at the interface of the above two categories: The idea of series expansion is also utilized in the CT-QMC method. Unlike CT-QMC, which resorts to diagrammatic perturbation ideas in many-body theory, our stochastic evaluation method is based on ansatz representation similar to those used in MCTDH. The proposed method is not restricted to a particular geometry of the systems, and is expected to work well when the stochastic ansatz captures the behavior of the physical system under study, as will be further illustrated by numerical examples. As another goal of the manuscript, we hope that the abstraction of the ideas developed in the physics and chemistry literature would help transferring these techniques for high dimensional computational challenges we face in other areas. Indeed, the unified framework of our method can be applied to any linear evolution problems in high dimensions.

## 2. Algorithm.

**2.1. Quantum kinetic Monte Carlo algorithm.** Before we turn to the specific quantum many-body spin dynamics, let us present the general framework of the algorithm. This is an abstraction of the ideas behind the surface hopping algorithms developed in our previous works [9, 1].

Given a Hamiltonian  $H$  on the Hilbert space  $\mathcal{H}$ , the quantum kinetic Monte Carlo algorithm starts with a choice of a decomposition of the Hamiltonian

$$(2.1) \quad H = H_{\text{easy}} + H_{\text{hard}},$$

together with a class of states  $\mathcal{A} \subset \mathcal{H}$ . We require that

- A) Any vector  $|\Psi\rangle \in \mathcal{A}$  is easy to represent (i.e., we do not need to store directly the full vector, but only a parametrized form of it). In general,  $\mathcal{A}$  might not be a vector space, i.e., the parametrization is nonlinear;
- B) For any  $|\Psi\rangle \in \mathcal{A}$ , the action of  $H_{\text{easy}}$  remains in  $\mathcal{A}$ :

$$(2.2) \quad e^{-itH_{\text{easy}}} |\Psi\rangle \in \mathcal{A}, \quad \forall t$$

and is easy to obtain (either exactly or with a controllable error);

- C) It is possible to stochastically represent the action of  $H_{\text{hard}}$ , in the sense that there exists a stochastic operator  $A(\omega)$  with  $\omega$  corresponding to some random space  $\Omega$ , such that for any  $|\Psi\rangle \in \mathcal{A}$ ,

$$(2.3) \quad \mathbb{E}_\omega A(\omega) |\Psi\rangle = H_{\text{hard}} |\Psi\rangle, \quad \text{and} \quad A(\omega) |\Psi\rangle \in \mathcal{A}, \quad \forall \omega.$$

In practice, it is often easier to first determine the set  $\mathcal{A}$ , and then look for the decomposition of the Hamiltonian and also the stochastic representation of the action of  $H_{\text{hard}}$ . Thus, in the following, when discussing two examples of algorithms developed under this framework, we will refer to them by the choice of the set  $\mathcal{A}$ .

With such a decomposition, the Schrödinger equation (1.5) can be written as the following integral form by the Duhamel's principle:

$$(2.4) \quad \begin{aligned} |\Psi(t)\rangle &= e^{-itH_{\text{easy}}} |\Psi(0)\rangle - i \int_0^t e^{-i(t-t_1)H_{\text{easy}}} H_{\text{hard}} |\Psi(t_1)\rangle dt_1 \\ &= e^{-itH_{\text{easy}}} |\Psi(0)\rangle - i \int_0^t \int_{\Omega} e^{-i(t-t_1)H_{\text{easy}}} A(\omega_1) |\Psi(t_1)\rangle d\mu_{\omega_1} dt_1, \end{aligned}$$

where we have used  $\mu_{\omega}$  to denote the probability measure of  $\omega$  and write

$$(2.5) \quad \mathbb{E}_{\omega} f(\omega) = \int_{\Omega} f(\omega) d\mu_{\omega}.$$

Note that the right hand side of (2.4) involves the unknown wave function at time  $t_1$ . To proceed, we apply (2.4) to its own right hand side and get

$$(2.6) \quad \begin{aligned} |\Psi(t)\rangle &= e^{-itH_{\text{easy}}} |\Psi(0)\rangle - i \int_0^t \int_{\Omega} e^{-i(t-t_1)H_{\text{easy}}} A(\omega_1) e^{-it_1 H_{\text{easy}}} |\Psi(0)\rangle d\mu_{\omega} dt_1 \\ &+ (-i)^2 \int_0^t \int_{\Omega} \int_0^{t_1} \int_{\Omega} e^{-i(t-t_1)H_{\text{easy}}} A(\omega_1) e^{-i(t_1-t_2)H_{\text{easy}}} A(\omega_2) |\Psi(t_2)\rangle d\mu_{\omega_2} dt_2 d\mu_{\omega_1} dt_1. \end{aligned}$$

Inserting again (2.4) into the right hand side of (2.6), we will get one more term on the right hand side. Such a substitution can be done repeatedly, which results into the following Dyson series expansion of  $|\Psi\rangle$ :

$$(2.7) \quad \begin{aligned} |\Psi(t)\rangle &= \sum_{M=0}^{+\infty} \int_0^t \int_{\Omega} \int_0^{t_1} \int_{\Omega} \cdots \int_0^{t_{M-1}} \int_{\Omega} (-i)^M \times \\ &\times e^{-i(t-t_1)H_{\text{easy}}} A(\omega_1) e^{-i(t_1-t_2)H_{\text{easy}}} A(\omega_2) \cdots \\ &\times e^{-i(t_{M-1}-t_M)H_{\text{easy}}} A(\omega_M) e^{-it_M H_{\text{easy}}} |\Psi(0)\rangle d\mu_{\omega_M} dt_M \cdots d\mu_{\omega_2} dt_2 d\mu_{\omega_1} dt_1 \\ &= \sum_{M=0}^{+\infty} \int_0^t \int_{\Omega} \int_0^{t_M} \int_{\Omega} \cdots \int_0^{t_2} \int_{\Omega} (-i)^M \times \\ &\times e^{-i(t-t_M)H_{\text{easy}}} A(\omega_M) e^{-i(t_M-t_{M-1})H_{\text{easy}}} A(\omega_{M-1}) \cdots \\ &\times e^{-i(t_2-t_1)H_{\text{easy}}} A(\omega_1) e^{-it_1 H_{\text{easy}}} |\Psi(0)\rangle d\mu_{\omega_1} dt_1 \cdots d\mu_{\omega_{M-1}} dt_{M-1} d\mu_{\omega_M} dt_M, \end{aligned}$$

where the last step is just renaming the integration variables. Using dominated convergence, it is easy to see that if the operators  $A(\omega)$  are uniformly bounded, the above series expansion converges absolutely. According to the properties B) and C), the integrand in the above equation is always a state in  $\mathcal{A}$ , and is therefore easy to represent. The challenge then lies in the high dimensional integration both in the stochastic space and in the time sequence, for which we turn to Monte Carlo method.

Before discussing the algorithm, let us note that the above can be extended to time-dependent Hamiltonian operators, with the assumption (2.3) now changes to for

any  $|\Psi\rangle \in \mathcal{A}$

$$(2.8) \quad \mathbb{E}_\omega A(t, \omega) |\Psi\rangle = H_{\text{hard}}(t) |\Psi\rangle, \quad \text{and} \quad A(t, \omega) |\Psi\rangle \in \mathcal{A},$$

and the semigroup generated by  $H_{\text{easy}}(t)$  preserves the state in  $\mathcal{A}$  (it is also possible to consider the more general case that the set  $\mathcal{A}$  depends on time). The expansion (2.7) changes to

$$(2.9) \quad \begin{aligned} |\Psi(t)\rangle = & \sum_{M=0}^{+\infty} \int_0^t \int_\Omega \int_0^{t_M} \int_\Omega \cdots \int_0^{t_2} \int_\Omega (-i)^M \times \\ & \times U(t, t_M) A(t_M, \omega_M) U(t_M, t_{M-1}) A(t_{M-1}, \omega_{M-1}) \cdots \\ & \times U(t_2, t_1) A(t_1, \omega_1) U(t_1, 0) |\Psi(0)\rangle \, d\mu_{\omega_1} dt_1 \cdots d\mu_{\omega_{M-1}} dt_{M-1} d\mu_{\omega_M} dt_M. \end{aligned}$$

with the unitary evolution operator  $U(t, s)$  given by

$$(2.10) \quad U(t, s) := \mathcal{T} \exp \left( -i \int_s^t H_{\text{easy}}(\tau) d\tau \right),$$

where  $\mathcal{T}$  is the time-ordering operator.

The expansion (2.9) inspires us to use Monte Carlo method to evaluate  $|\Psi(t)\rangle$ . In such a method, each sample would be the integrand on the right hand side of (2.9). To determine the integrand, we need to specify the following:

1. A non-negative integer  $M$ ;
2. A sequence of random times:  $0 \leq t_1 \leq t_2 \leq \cdots \leq t_M \leq t$ ;
3. A sequence of random samples in  $\Omega$ :  $\omega_1, \cdots, \omega_M$ .

This links the Monte Carlo method to a marked point process with mark space  $\Omega$  (see the textbook [8] for an introduction of the marked point process and also point process in general). We denote  $\Xi = ((t_m), (\omega_m))_{m \geq 1}$  one realization of the marked point process, in which  $\omega_m \in \Omega$  is marked at time  $t_m$ . The marked point process is generated by an intensity function  $\lambda(t, \omega)$ , *i.e.*

$$(2.11) \quad \mathbb{P}(\text{A mark in } \Sigma \text{ appears in } [t, t+h]) = \int_\Sigma \lambda(t, \omega) h \, d\mu_\omega + o(h), \quad \forall t > 0, \quad \forall \Sigma \subset \Omega.$$

Any intensity function that is strictly positive can be used, a better choice will however reduce the sampling variance of the algorithm. We will further discuss the choice of the intensity function in the next section.

The following identity is essential to our method: It turns the problem of calculating  $|\Psi(t)\rangle$  into a sampling problem:

$$(2.12) \quad |\Psi(t)\rangle = \mathbb{E}_\Xi |\Phi_\Xi(t)\rangle,$$

if for a given realization of the marked point process  $\Xi$ , the state  $|\Phi_\Xi(t)\rangle$  is defined by

$$(2.13) \quad \begin{aligned} |\Phi_\Xi(t)\rangle = & \exp \left( \int_0^t \int_\Omega \lambda(s, \omega) \, d\mu_\omega \, ds \right) U(t, t_M) \tilde{A}(t_M, \omega_M) \times \\ & \times U(t_M, t_{M-1}) \tilde{A}(t_{M-1}, \omega_{M-1}) \cdots U(t_2, t_1) \tilde{A}(t_1, \omega_1) U(t_1, 0) |\Psi(0)\rangle, \end{aligned}$$

where  $M$  is the number of marks in  $\Xi$  before time  $t$ , and we have used the short hands

$$(2.14) \quad \tilde{A}(t_m, \omega_m) = -iA(t_m, \omega_m)/\lambda(t_m, \omega_m), \quad m = 1, \dots, M.$$

The equality (2.12) follows as for any function  $\mathcal{F}(\Xi)$  depending only on the part of  $\Xi$  in the time interval  $[0, t)$ , we have

$$(2.15) \quad \begin{aligned} \mathbb{E}_\Xi \mathcal{F}(\Xi) &= \sum_{M=0}^{+\infty} \int_0^t \int_\Omega \int_0^{t_M} \int_\Omega \cdots \int_0^{t_2} \int_\Omega \exp\left(-\int_0^t \int_\Omega \lambda(s, \omega) d\mu_\omega ds\right) \times \\ &\quad \times \left(\prod_{m=1}^M \lambda(t_m, \omega_m)\right) \mathcal{F}(\Xi) d\mu_{\omega_1} dt_1 \cdots d\mu_{\omega_{M-1}} dt_{M-1} d\mu_{\omega_M} dt_M. \end{aligned}$$

An algorithm to evaluate  $|\Psi(t)\rangle$  naturally follows the equality (2.12). The idea is to draw a sequence of realizations of process  $\Xi$ , evaluate  $|\Phi_\Xi(t)\rangle$  for each realization, an estimate of  $|\Psi\rangle$  is then given by the average. For easier implementation, we define

$$(2.16) \quad \eta(t) = \int_0^t \int_\Omega \lambda(s, \omega) d\mu_\omega ds, \quad |\tilde{\Phi}_\Xi(t)\rangle = e^{-\eta(t)} |\Phi_\Xi(t)\rangle.$$

It can be easily seen that  $\eta(t)$  can be obtained by solving

$$(2.17) \quad \frac{d\eta}{dt} = \int_\Omega \lambda(t, \omega) d\mu_\omega.$$

Thus, while evolving the state  $|\Phi_\Xi(t)\rangle$ , an additional scalar quantity  $\eta(t)$  needs to be evolved simultaneously. In our application, the mark space  $\Omega$  is a finite set, and therefore solving (2.17) does not introduce much numerical cost. In (2.16), the time-dependent state  $|\tilde{\Phi}_\Xi(t)\rangle$  can be considered as a trajectory in  $\mathcal{A}$ . To obtain this trajectory, we use the fact that between two adjacent marks, the trajectory satisfies

$$(2.18) \quad \frac{d}{dt} |\tilde{\Phi}_\Xi(t)\rangle = -iH_{\text{easy}}(t) |\tilde{\Phi}_\Xi(t)\rangle, \quad t \in (t_{m-1}, t_m), \quad m > 0.$$

When a mark is met, one just needs to apply the operator  $\tilde{A}(t_m, \omega_m)$ . An illustration of the trajectory  $|\tilde{\Phi}_\Xi(t)\rangle$  is given in Figure 2.1.

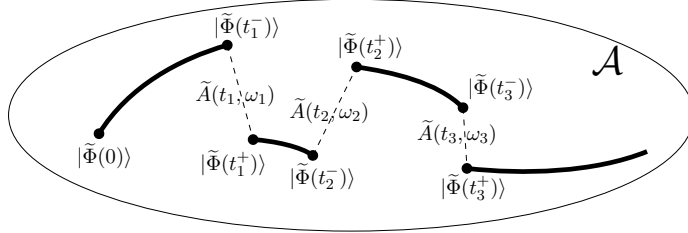


Fig. 2.1: Illustration of the trajectory  $|\tilde{\Phi}_\Xi(t)\rangle$ . The bold lines denote the evolution of the equation (2.18), and the thin dashed lines denote the application of the operator marked over them. The states  $|\tilde{\Phi}_\Xi(t_k^\pm)\rangle$  are the left/right limits of  $|\tilde{\Phi}_\Xi(t)\rangle$  at  $t_k$ .

In (2.16), the reason for introducing  $\eta(t)$  is the following property:

$$(2.19) \quad \mathbb{P}(\text{no mark exists in } (s_1, s_2)) = \exp(-[\eta(s_2) - \eta(s_1)]),$$

which helps us to realize the marked point process. In our implementation, the drawing of the marked point process and the evolution of the trajectory are simultaneously done. In detail, one trajectory  $|\tilde{\Phi}_\Xi(t)\rangle$  can be obtained by the following steps:

1. Set  $t \leftarrow 0$ ,  $\tilde{\eta} \leftarrow 0$ ,  $|\tilde{\Phi}_\Xi(0)\rangle \leftarrow |\Psi(0)\rangle$ ,  $flag \leftarrow false$ . Generate a random number  $Y$  obeying the uniform distribution in  $[0, 1]$ .
2. Stop if  $t$  is large enough. Otherwise, select a time step  $\Delta t$ , and solve  $\eta(t + \Delta t)$  according to (2.17).
3. If  $\exp(\tilde{\eta} - \eta(t + \Delta t)) \leq 1 - Y$ , then solve the equation of the mark time  $\tilde{t}$

$$\exp(\tilde{\eta} - \eta(\tilde{t})) = 1 - Y$$

by interpolation of  $\eta(t)$  in  $[t, t + \Delta t]$ , and set  $\Delta t \leftarrow \tilde{t} - t$ ,  $flag \leftarrow true$ ,  $\tilde{\eta} = \eta(\tilde{t})$ .

4. Solve the equation (2.18) to get  $|\tilde{\Phi}_\Xi(t + \Delta t)\rangle$ . Set  $t \leftarrow t + \Delta t$ .
5. If  $flag$  is *false*, return to step 2. Otherwise, generate a mark  $\omega \in \Omega$  according to the probability measure  $\mu_\omega$ , and set  $|\tilde{\Phi}_\Xi(t)\rangle \leftarrow \tilde{A}(t, \omega)|\tilde{\Phi}_\Xi(t)\rangle$ . Generate a new uniformly distributed random variable  $Y \in [0, 1]$  and return to step 2.

In the above algorithm,  $\tilde{\eta}$  records the value of  $\eta$  at the last mark, and step 3 uses the property (2.19) to determine the time of the next mark. When a mark is set at the current time step, the boolean variable  $flag$  is set to be true, and in step 5, a mark is picked from the mark space. By doing this, the whole process  $\Xi$  is generated mark by mark. At the same time, the value of  $\eta(t)$  at the trajectory  $|\tilde{\Phi}_\Xi(t)\rangle$  is obtained at all discrete times, and thus  $|\Phi_\Xi(t)\rangle$  can be evaluated by  $|\Phi_\Xi(t)\rangle = e^{\eta(t)}|\tilde{\Phi}_\Xi(t)\rangle$ . Regarding the computational cost, it can be seen that at each time step for a single trajectory, we need to evaluate the integral over  $\Omega$  for  $O(1)$  times (depends on the Runge-Kutta method used), apply  $H_{\text{easy}}$  for  $O(1)$  times, and apply  $\tilde{A}(t, \omega)$  at most once.

REMARK 2.1. *This section gives a general framework for the algorithm. To apply the algorithm, we need a decomposition (2.1) satisfying the conditions A) to C). In general, such decomposition should be studied case by case. One standard way is to decompose the Hamiltonian into non-interacting and interacting parts, where the non-interacting part will be regarded as  $H_{\text{easy}}$  and the interacting part as  $H_{\text{hard}}$ . Since the interacting part usually induces many-body entanglement to the system and is therefore considered as “hard”.*

**2.2. QKMC with Z-basis.** Let us now consider specific examples of the quantum kinetic Monte Carlo algorithm. In the first example, we take

$$(2.20) \quad \mathcal{A} = \left\{ |\Psi\rangle = a |\psi_1\rangle \otimes \cdots \otimes |\psi_N\rangle \mid a \in \mathbb{C}, |\psi_i\rangle \in \{|\uparrow\rangle, |\downarrow\rangle\}, \forall i \right\}$$

We call this the Z-basis, since each  $|\Psi\rangle \in \mathcal{A}$  is an eigenvector of (one-body or many-body) Pauli matrices in the z-direction.

It is obvious that we can choose  $H_{\text{easy}}$  as

$$(2.21) \quad H_{\text{easy}}(t) = \sum_{k=1}^N m_3^{(k)} \sigma_3^{(k)} + \sum_{1 \leq j < k \leq N} \gamma_{jk}(t) \sigma_3^{(j)} \sigma_3^{(k)},$$

since for  $U(t, s)$  defined as (2.10),

$$(2.22) \quad U(t, s) |\Psi\rangle = \exp \left( -i(t-s) \sum_{k=1}^N \kappa_k m_3^{(k)} - i \sum_{1 \leq j < k \leq N} \kappa_j \kappa_k \int_s^t \gamma_{jk}(\tau) d\tau \right) |\Psi\rangle,$$

where  $|\Psi\rangle$  is an arbitrary state in  $\mathcal{A}$  and  $\kappa_k = \langle \psi_k | \sigma_3 | \psi_k \rangle$ . The sample space for  $\omega$  can be chosen as  $\Omega = \Omega_1 \cup \Omega_2$ , where

$$(2.23) \quad \Omega_1 = \{k \mid k = 1, \dots, N\}, \quad \Omega_2 = \{(j, k) \mid j, k = 1, \dots, N, j < k\},$$

and the operator  $A(t, \omega)$  is set to be

$$(2.24) \quad A(t, \omega) = \begin{cases} |\Omega| (m_1^{(k)} \sigma_1^{(k)} + m_2^{(k)} \sigma_2^{(k)}), & \text{if } \omega = k \in \Omega_1, \\ |\Omega| \gamma_{jk}(t) (\sigma_1^{(j)} \sigma_1^{(k)} + \sigma_2^{(j)} \sigma_2^{(k)}), & \text{if } \omega = (j, k) \in \Omega_2, \end{cases}$$

where  $|\Omega| = N(N+1)/2$  is the cardinality of  $\Omega$ . For all  $\omega_0 \in \Omega$ , the probabilities are assigned the same:

$$(2.25) \quad \mathbb{P}(\omega = \omega_0) = \frac{1}{|\Omega|},$$

which gives the definition of  $\mu_\omega$ . The above definitions immediately lead to

$$(2.26) \quad \mathbb{E}_\omega A(t, \omega) = H_{\text{hard}} := H - H_{\text{easy}}.$$

In our implementation, the intensity function  $\lambda(t, \omega)$  is chosen as

$$(2.27) \quad \lambda(t, \omega) = \begin{cases} |\Omega| |m_1^{(k)} + i m_2^{(k)}| & \text{if } \omega = k \in \Omega_1, \\ 2|\Omega| |\gamma_{jk}(t)| & \text{if } \omega = (j, k) \in \Omega_2, \end{cases}$$

so that the operator  $\tilde{A}(t, \omega)$  defined in (2.14) does not change the magnitude of the state.

REMARK 2.2. *The Z-basis can be considered as a weight multiplied by an element in the finite set*

$$(2.28) \quad \mathcal{S} = \left\{ |\psi_1\rangle \otimes \dots \otimes |\psi_N\rangle \mid |\psi_i\rangle \in \{|\uparrow\rangle, |\downarrow\rangle\}, \forall i \right\}.$$

*From this point of view, the marked point process can be interpreted as a jump process with state space  $\mathcal{S}$ . In detail, supposing the current state in the jump process is  $|\Psi\rangle$ , we can interpret the mark  $\omega$  at time  $t$  as the jump  $|\Psi\rangle \rightarrow |\Phi\rangle$ , where  $|\Phi\rangle$  is the only state in  $\mathcal{S}$  such that  $\langle \Phi | A(t, \omega) | \Psi \rangle \neq 0$ . At each jump, the weight is changed to fit the result of applying  $\tilde{A}(t, \omega)$ . Such an interpretation matches the currently proposed method with the surface hopping method proposed in [1], where each element in  $\mathcal{S}$  is considered as a “surface”, and the weight is considered as evolving on the surfaces.*

**2.3. QKMC with simple tensors.** In this case, we choose the subset  $\mathcal{A}$  to be all simple tensors in the tensor product space  $\mathcal{H} = (\mathbb{C}^2)^{\otimes N}$ .

$$(2.29) \quad \mathcal{A} = \left\{ |\Psi\rangle = |\psi_1\rangle \otimes \dots \otimes |\psi_N\rangle \mid |\psi_i\rangle \in \mathbb{C}^2, \forall i \right\}$$

It is clear that this set is larger than the one of Z-basis.



In such a case, we can choose  $H_{\text{easy}}$  to be

$$(2.30) \quad H_{\text{easy}}(t) = \sum_{k=1}^N m^{(k)}(t) \cdot \sigma^{(k)}.$$

Thus for any  $|\Psi\rangle = |\psi_1\rangle \otimes \cdots \otimes |\psi_N\rangle \in \mathcal{A}$ , we have

$$U(t, s) |\Psi\rangle = U^{(1)}(t, s) |\psi_1\rangle \otimes \cdots \otimes U^{(N)}(t, s) |\psi_N\rangle \in \mathcal{A},$$

where

$$U^{(k)}(t, s) = \exp\left(-i \left[ \int_s^t m^{(k)}(\tau) d\tau \right] \cdot \sigma\right),$$

where  $\sigma = (\sigma_1, \sigma_2, \sigma_3)^\top$ . The sample space  $\Omega$  and the probability measure  $\mu_\omega$  are given by

$$(2.31) \quad \Omega = \{(i, j, k) \mid i = 1, 2, 3, j, k = 1, \dots, N, j < k\}, \quad \mathbb{P}(\omega = \omega_0) = 1/|\Omega|, \quad \forall \omega_0 \in \Omega.$$

By defining

$$(2.32) \quad A(t, \omega) = |\Omega| \gamma_{jk}(t) \sigma_i^{(j)} \sigma_i^{(k)},$$

it is easy to find that  $\mathbb{E}_\omega A(t, \omega) = H(t) - H_{\text{easy}}(t)$ . Again, we choose

$$(2.33) \quad \lambda(t, \omega) = |\Omega| |\gamma_{jk}(t)|,$$

so that  $\tilde{A}(t, \omega)$  does not change the norm of the state.

In this method, the evolution equation for  $\eta(t)$  defined in (2.16) is

$$(2.34) \quad \frac{d\eta}{dt} = 3 \sum_{1 \leq j < k \leq N} |\gamma_{jk}(t)|.$$

In the method using  $Z$ -basis (see Section 2.2), we have

$$(2.35) \quad \frac{d\eta}{dt} = \sum_{k=1}^N |m_1^{(k)} + im_2^{(k)}| + 2 \sum_{1 \leq j < k \leq N} |\gamma_{jk}(t)|.$$

Therefore, if the coupling intensity is significantly smaller than the control field, the growing rate of  $\eta(t)$  in (2.35) is larger than that in (2.34), which indicates larger variance in the numerical solution with  $Z$ -basis.

**3. Analysis of the sampling variance.** In this section, we discuss the evolution of the numerical error for the above algorithm. Suppose  $N_{\text{traj}}$  trajectories are used in the simulation. Then the numerical solution is

$$(3.1) \quad |\Psi_{\text{num}}(t)\rangle = \frac{1}{N_{\text{traj}}} \sum_{i=1}^{N_{\text{traj}}} |\Phi_{\Xi_i}(t)\rangle,$$

where  $\Xi_i$  is the realization of the marked point process corresponding to the  $i$ -th trajectory, and  $\Xi_i$  and  $\Xi_j$  are independent of each other if  $i \neq j$ . Define  $|\Psi_{\text{err}}(t)\rangle$  as the difference between the numerical solution and the exact solution:

$$(3.2) \quad |\Psi^{\text{err}}(t)\rangle = |\Psi^{\text{num}}(t)\rangle - |\Psi(t)\rangle.$$

Apparently  $\mathbb{E} |\Psi^{\text{err}}(t)| = 0$ . Therefore the variance of  $|\Psi^{\text{err}}(t)|$  is

$$(3.3) \quad \sigma^2 = \mathbb{E} \langle \Psi^{\text{err}}(t) | \Psi^{\text{err}}(t) \rangle,$$

which will be estimated below.

Inserting (3.1) and (3.2) into (3.3) and using the fact that  $\mathbb{E}_{\Xi_i} |\Phi_{\Xi_i}(t)| = |\Psi(t)|$  for any  $i$ , we have

$$(3.4) \quad \sigma^2 = \frac{1}{N_{\text{traj}}^2} \sum_{i=1}^{N_{\text{traj}}} \sum_{j=1}^{N_{\text{traj}}} \mathbb{E}_{\Xi_i, \Xi_j} \langle \Phi_{\Xi_i}(t) | \Phi_{\Xi_j}(t) \rangle - \langle \Psi(t) | \Psi(t) \rangle.$$

Since all trajectories are independent, in the above sum, the terms with  $i \neq j$  can be directly evaluated, which yields

$$(3.5) \quad \sigma^2 = \frac{1}{N_{\text{traj}}} \mathbb{E}_{\Xi} \langle \Phi_{\Xi}(t) | \Phi_{\Xi}(t) \rangle - \frac{1}{N_{\text{traj}}} \langle \Psi(t) | \Psi(t) \rangle.$$

This equation shows that the the variance is proportional to the inverse of the number of trajectories, which is of course typical for Monte Carlo algorithms.

To further estimate  $\mathbb{E}_{\Xi} \langle \Phi_{\Xi}(t) | \Phi_{\Xi}(t) \rangle$ , we use the definition of the trajectory (2.13) to get

$$(3.6) \quad \langle \Phi_{\Xi}(t) | \Phi_{\Xi}(t) \rangle \leq \exp \left( 2 \int_0^t \int_{\Omega} \lambda(s, \omega) d\mu_{\omega} ds \right) \left( \prod_{m=1}^M \|\tilde{A}(t_m, \omega_m)\| \right)^2 \langle \Psi(0) | \Psi(0) \rangle,$$

where  $\|\cdot\|$  is the operator norm, and we have used the fact that  $U(\cdot, \cdot)$  is a unitary operator. If the intensity function  $\lambda(t, \omega)$  is chosen such that there exist constants  $\Lambda$  and  $\tilde{\alpha}$  satisfying

$$(3.7) \quad |\lambda(t, \omega)| \leq \Lambda \quad \text{and} \quad \|\tilde{A}(t, \omega)\| \leq \tilde{\alpha}, \quad \forall t \in \mathbb{R}^+, \quad \forall \omega \in \Omega,$$

we can apply (2.15) to get

$$(3.8) \quad \mathbb{E}_{\Xi} \langle \Phi_{\Xi}(t) | \Phi_{\Xi}(t) \rangle \leq e^{\Lambda t} \langle \Psi(0) | \Psi(0) \rangle \sum_{M=0}^{+\infty} \frac{t^M}{M!} \Lambda^M \tilde{\alpha}^{2M} = e^{\Lambda(1+\tilde{\alpha}^2)t} \langle \Psi(0) | \Psi(0) \rangle.$$

Here one sees that the variance grows exponentially with respect to  $t$ .

Note that the equation (3.6) becomes an equality if every operator  $A(t, \omega)$  is a unitary operator multiplied by a positive constant  $\alpha$ . This condition holds for (2.32) if we have either  $\gamma_{jk}(t) \equiv 0$  or  $\gamma_{jk}(t) \equiv \gamma$  for any  $j, k$ , and in this case, we have  $\alpha = \|A(t, \omega)\| = N_c \gamma$ , where  $N_c$  is the number of the pairs of coupling spins, i.e. the number of  $\gamma_{jk}$  which are not zero. Since  $\|\tilde{A}(t, \omega)\| = \|A(t, \omega)\|/\lambda(t, \omega) = \alpha/\lambda(t, \omega)$ , we need a lower bound of  $\lambda(t, \omega)$  to get a finite  $\tilde{\alpha}$  as defined in (3.7). Assume  $\lambda(t, \omega) \geq \ell$ , and then the estimation (3.8) becomes

$$(3.9) \quad \mathbb{E}_{\Xi} \langle \Phi_{\Xi}(t) | \Phi_{\Xi}(t) \rangle \leq e^{t\Lambda[1+(\alpha/\ell)^2]} \langle \Psi(0) | \Psi(0) \rangle.$$

Using the inequality

$$(3.10) \quad \Lambda[1+(\alpha/\ell)^2] \geq \Lambda[1+(\alpha/\Lambda)^2] \geq 2\alpha,$$

we get a minimum value for the right hand side of (3.9), which can be achieved when  $\lambda(t, \omega) \equiv \ell = \Lambda = \alpha$ . Such a choice also turns (3.8) and (3.9) into equalities, and we eventually have

$$(3.11) \quad \mathbb{E}_{\Xi} \langle \Phi_{\Xi}(t) | \Phi_{\Xi}(t) \rangle = e^{2\alpha t} \langle \Psi(0) | \Psi(0) \rangle.$$

In fact, we can also show in this case that the variance is minimized by choosing  $\lambda(t, \omega) \equiv \alpha$ . To simplify the notation, we define

$$(3.12) \quad w_{\Xi}(t) = \exp \left( \int_0^t \int_{\Omega} \lambda(s, \omega) d\mu_{\omega} ds \right) \prod_{m=1}^M \frac{\alpha}{\lambda(t_m, \omega_m)}.$$

Then  $\langle \Phi_{\Xi}(t) | \Phi_{\Xi}(t) \rangle = [w_{\Xi}(t)]^2 \langle \Psi(0) | \Psi(0) \rangle$ . Applying (2.15) to  $w_{\Xi}(t)$  yields  $\mathbb{E}_{\Xi} w_{\Xi}(t) = e^{\alpha t}$ , and thus we get the following estimation of the lower bound:

$$(3.13) \quad \begin{aligned} \mathbb{E}_{\Xi} \langle \Phi_{\Xi}(t) | \Phi_{\Xi}(t) \rangle &= \langle \Psi(0) | \Psi(0) \rangle \mathbb{E}_{\Xi} [w_{\Xi}(t)]^2 \\ &\geq \langle \Psi(0) | \Psi(0) \rangle [\mathbb{E}_{\Xi} w_{\Xi}(t)]^2 = e^{2\alpha t} \langle \Psi(0) | \Psi(0) \rangle. \end{aligned}$$

From (3.11), it is clear that  $\lambda(t, \omega) = \alpha$  gives the optimal intensity function.

The above analysis also explains the reason for our choice (2.33). When  $\gamma_{jk}(t)$  is either zero or a fixed constant  $\gamma$  as stated in the beginning of the previous paragraph, we can naturally remove the tuples  $(i, j, k)$  with  $\gamma_{jk}(t) \equiv 0$  from the sample space  $\Omega$  defined in (2.31), and then  $|\Omega| = N_c$  and (2.33) becomes  $\lambda(t, \omega) = N_c \gamma = \alpha$ , which gives exactly the optimal intensity function.

## 4. Numerical results.

**4.1. Examples with few spins: Validity check.** To verify the algorithm, we first consider some simple cases with only a few spins. The magnetic field  $(m_1(t), m_2(t))$  is chosen as

$$m_1(t) = \cos(\omega t), \quad m_2(t) = \sin(\omega t)$$

with  $\omega = -0.5$ , and  $m_3^{(k)} = 1$  is used for all the spins. Assuming that each spin interacts only with its adjacent spins, and all the interaction strengths are equal, we have that

$$\gamma_{jk}(t) = \gamma_0 \delta_{1, |j-k|}.$$

Initially, we assume that all the spins have the same state  $|\uparrow\rangle$ :

$$(4.1) \quad |\Psi(0)\rangle = |\uparrow\rangle^{\otimes N},$$

and we are concerned about the evolution of the probability for the “all spin-down” state:

$$(4.2) \quad p(t) = \langle \Psi(t) | B | \Psi(t) \rangle, \quad B = |\Psi_{\text{down}}\rangle \langle \Psi_{\text{down}}|,$$

where  $|\Psi_{\text{down}}\rangle = |\downarrow\rangle^{\otimes N}$ . For small  $N$ , we use a deterministic Runge-Kutta solver to provide reference solutions.

In Figure 4.1, we show the numerical results using QKMC with  $Z$ -basis. The cases with one spin to four spins are considered, and the coupling intensity  $\gamma_0$  is set to be 0.05. For all the four cases, 1,000,000 trajectories are used. It can be seen that when  $t$  is large, the numerical solution of QKMC becomes oscillatory and unreliable,

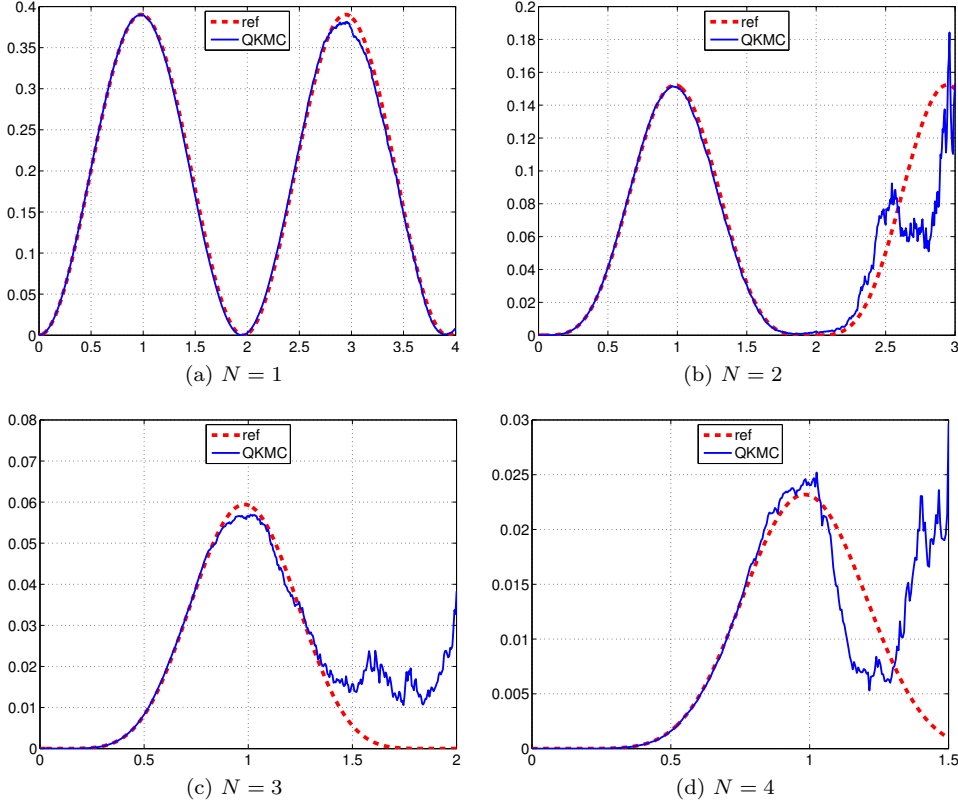


Fig. 4.1: Numerical tests of QKMC with Z-basis,  $\gamma_0 = 0.05$

due to the large sample variance. As the number of spins increases, the reliable part of the curve becomes shorter.

Better results can be obtained using the QKMC with simple tensors. Figure 4.2 shows the numerical results with the same settings. The number of trajectories is again 1,000,000. For this method, when only one spin is present, the algorithm is identical to the deterministic ODE solver. In all the four cases, two complete cycles are obtained without obvious oscillation.

In the case of 4 spins, we also check the numerical error for QKMC with simple tensors. Using the result of the deterministic solver as the reference solution  $|\Psi^{\text{ref}}(t)\rangle$ , we plot the evolution of the 2-norm of numerical error  $|\Psi^{\text{err}}(t)\rangle = |\Psi^{\text{num}}(t)\rangle - |\Psi^{\text{ref}}(t)\rangle$ :

$$(4.3) \quad e_{N_{\text{traj}}}(t) = \sqrt{\langle \Psi^{\text{err}}(t) | \Psi^{\text{err}}(t) \rangle},$$

where  $|\Psi^{\text{num}}(t)\rangle$  is the numerical solution of QKMC with  $N_{\text{traj}}$  trajectories. Figure 4.3 shows the reduction of the error as the number of trajectories increases, and the order of convergence is calculated in Figure 4.4. It is obvious that the numerical order is around 1/2 for all  $t$ , which indicates that the expected convergence rate in the Monte Carlo method is achieved in our numerical test.

**4.2. High dimensional tests.** The cases with more spins are shown in Figure 4.5. Here we consider weaker coupling intensity  $\gamma_0 = 0.01$ , while the number of spins

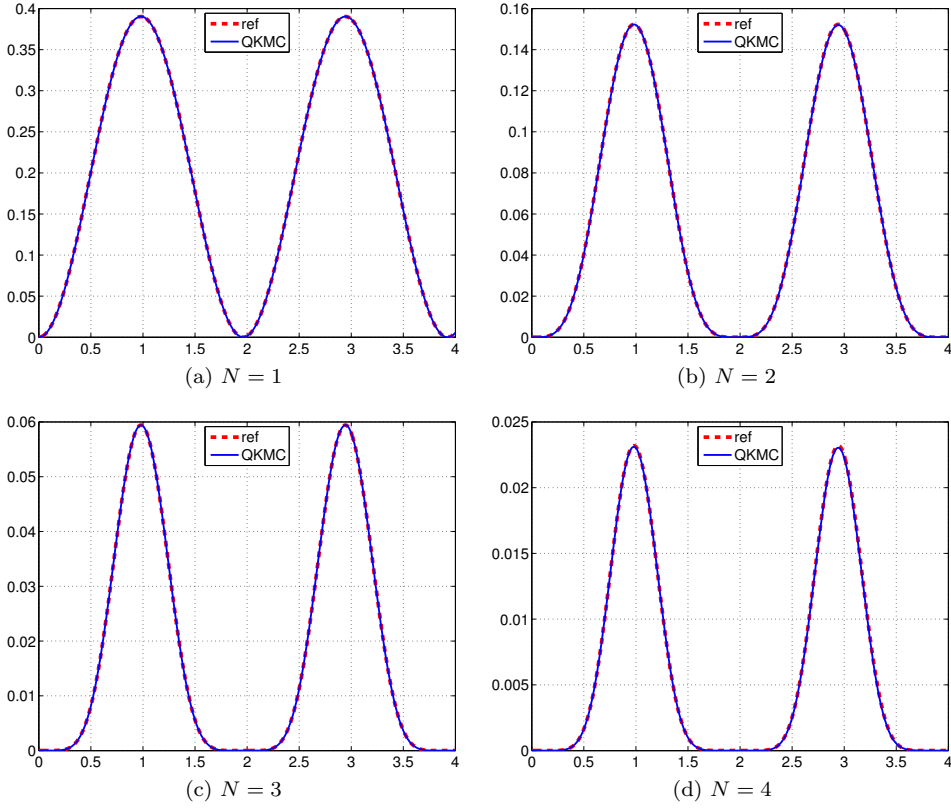


Fig. 4.2: Numerical tests of QKMC with simple tensors,  $\gamma_0 = 0.05$

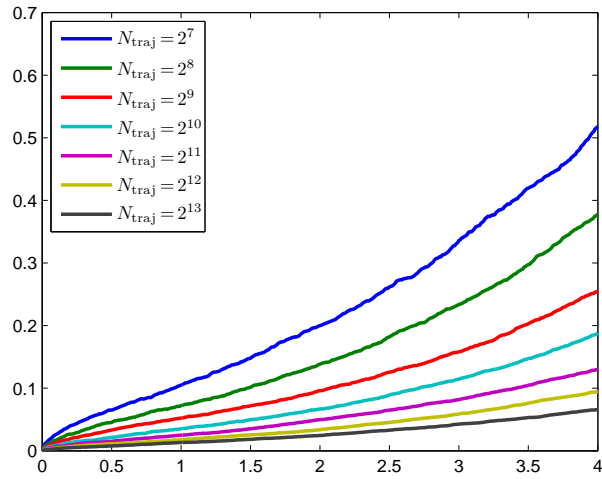


Fig. 4.3: Evolution of the numerical error  $e_{N_{\text{traj}}}$  (defined in (4.3)) for 4 spins. The  $x$ -axis is the time  $t$ , and the  $y$ -axis is the 2-norm error of the solution.

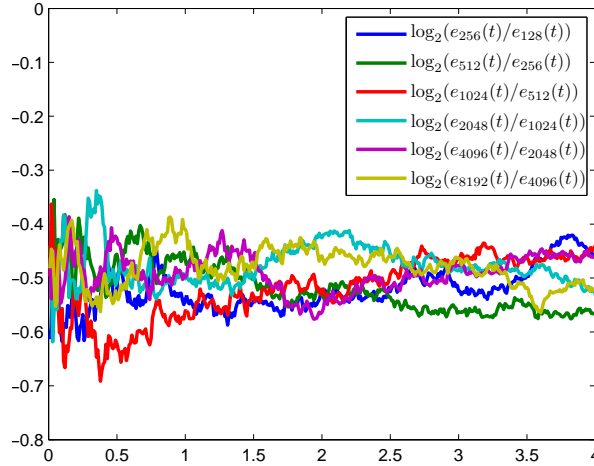


Fig. 4.4: Evolution of the numerical order for 4 spins. The  $x$ -axis is the time  $t$ , and the  $y$ -axis is the numerical order obtained as indicated in the legend.

ranges from 10 to 40. In these cases, the method with  $Z$ -basis needs a huge number of trajectories to get meaningful results, which is out of our current computational capacity. However, by using 8,000,000 trajectories, two complete cycles are still well obtained using QKMC with simple tensors. For 10 and 20 spins, the numerical results are again validated by comparison with the reference results. For 30 and 40 spins, the reference solutions are not provided since the computational time for a deterministic solver is not affordable. For the case of 40 spins, the second peak is lower than the first one, which might indicate some numerical error induced by insufficient number of trajectories.

**4.3. Numerical examples with random parameters.** In this example, we assume that the interactions and the energy splittings are random. For spin interactions, we let  $\mathcal{I}_c$  be the set of all possible interaction pairs:

$$(4.4) \quad \mathcal{I}_c = \{(j, k) \mid 1 \leq j < k \leq N\}.$$

For each trajectory, we randomly pick a subset  $\mathcal{I} \subset \mathcal{I}_c$  with  $N - 1$  elements. Using  $U(a, b)$  to denote the uniform distribution in  $[a, b]$ , we set the coupling intensity to be

$$(4.5) \quad \gamma_{jk}(t) \begin{cases} \sim U(\gamma_0 - \Delta\gamma, \gamma_0 + \Delta\gamma), & \text{if } (j, k) \in \mathcal{I}, \\ = 0, & \text{otherwise.} \end{cases}$$

The energy splitting  $m_3^{(k)}$  is also assumed to be uniformly distributed:

$$(4.6) \quad m_3^{(k)} \sim U(0.9, 1.1).$$

The initial condition is the same as (4.1).

Figure 4.6 shows the results of  $p(t)$  with  $\gamma_0 = 0.05$  and  $\Delta\gamma = 0.005$  for one to four spins, and the number of trajectories is again 1,000,000. Different from the deterministic cases in Section 4.1, the second peak is slightly lower than the first peak, which indicates some cancellation between different interaction patterns. Similarly, we also consider the case with weaker coupling intensity  $\gamma_0 = 0.01$ ,  $\Delta\gamma = 0.001$  but more

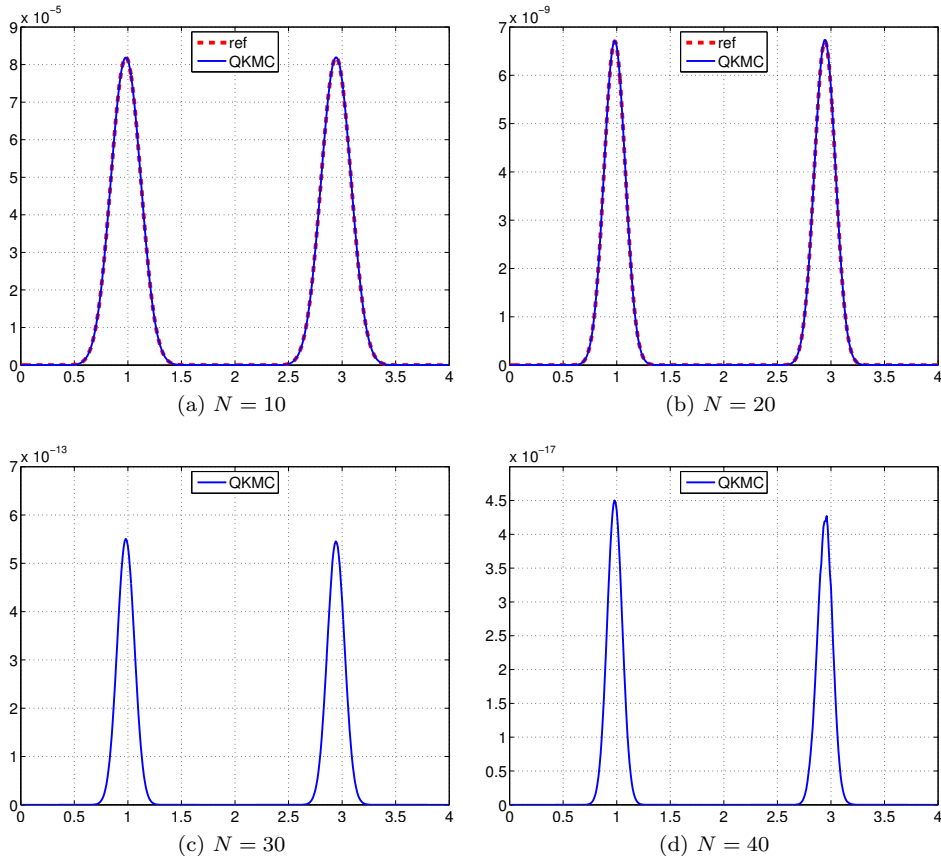


Fig. 4.5: Numerical tests of QKMC with simple tensors,  $\gamma_0 = 0.01$

spins. Smooth results can be obtained with 8,000,000 trajectories for as many as 40 spins. Figure 4.7 also shows the lower second peaks, which indicates the qualitatively correct behavior of the numerical solution.

**5. Conclusion.** In this work, we propose a stochastic method to solve the multi-spin dynamics. The method is derived from a quite general framework and the multi-spin dynamics appears here to be an interesting application. Numerical experiments show that very small “flipping probabilities” can be well captured by this method in a system with as many as 40 spins. Future work includes other applications of this framework and numerical techniques reducing the variance in the solution and better preserving the conservative quantities.

#### REFERENCES

- [1] Z. CAI AND J. LU, *A surface hopping Gaussian beam method for high-dimensional transport systems*, 2017. preprint, arXiv:1703.06116.
- [2] G. COHEN, E. GULL, D. R. REICHMAN, AND A. J. MILLIS, *Taming the dynamical sign problem in real-time evolution of quantum many-body problems*, Phys. Rev. Lett., 115 (2015), p. 266802.

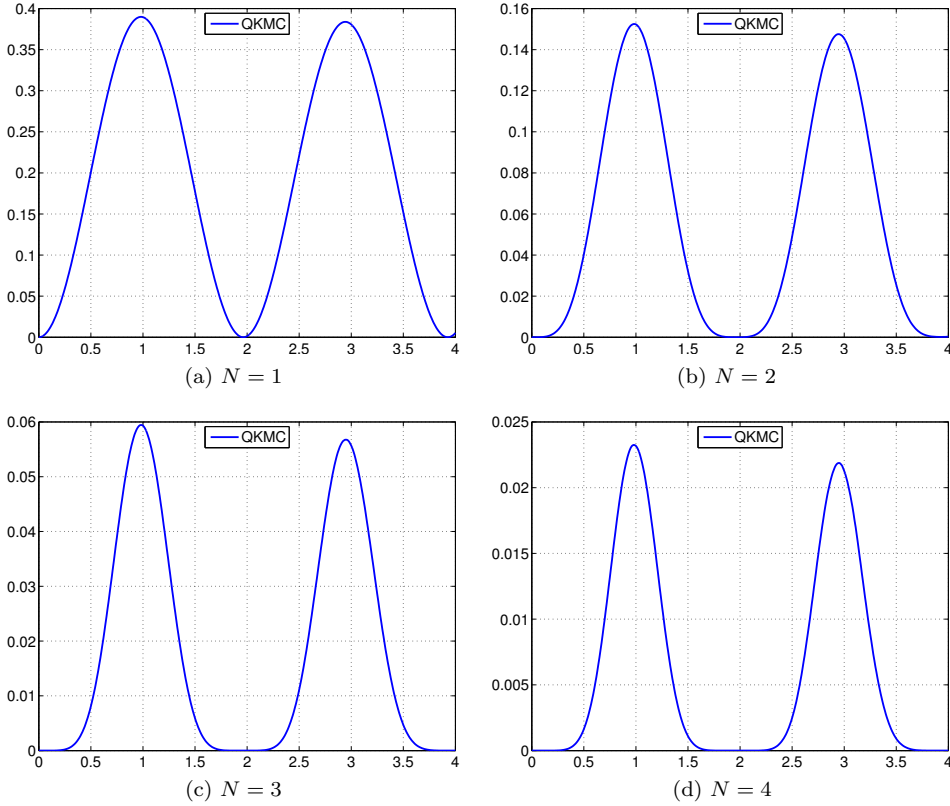


Fig. 4.6: Numerical tests with randomness,  $\gamma_0 = 0.05$

- [3] R. R. ERNST, G. BODENHAUSEN, AND A. WOKAUN, *Principles of Nuclear Magnetic Resonance in One and Two Dimensions*, Clarendon Press, 1990.
- [4] G. FRIESECKE, F. HENNEKE, AND K. KUNISCH, *Sparse control of quantum systems*, 2015. preprint, arXiv:1507.00768.
- [5] E. GULL, A. MILLIS, A. LICHTENSTEIN, A. RUBTSOV, M. TROYER, AND P. WERNER, *Continuous-time Monte Carlo methods for quantum impurity models*, *Rev. Mod. Phys.*, 83 (2011), pp. 349–404.
- [6] J. E. HIRSCH AND R. M. FYE, *Monte Carlo method for magnetic impurities in metals*, *Phys. Rev. Lett.*, 56 (1986), p. 2521.
- [7] J. HUBBARD, *Calculation of partition functions*, *Phys. Rev. Lett.*, 3 (1959), p. 77.
- [8] M. JACOBSEN, *Point Process Theory and Applications*, Probability and Its Applications, Birkhäuser Basel, 2006.
- [9] J. LU AND Z. ZHOU, *Frozen Gaussian approximation with surface hopping for mixed quantum-classical dynamics: A mathematical justification of fewest switches surface hopping algorithms*, *Math. Comp.*, in press. arXiv:1602.06459.
- [10] H. D. MEYER, U. MANTHE, AND L. S. CEDERBAUM, *The multi-configurational time-dependent Hartree approach*, *Chem. Phys. Lett.*, 165 (1990), p. 73.
- [11] L. MUHLBACHER AND E. RABANI, *Real-time path integral approach to nonequilibrium many-body quantum systems*, *Phys. Rev. Lett.*, 100 (2008), p. 176403.
- [12] N. V. PROKOF'EV, B. V. SVISTUNOV, AND I. S. TUPITSYN, *Exact quantum Monte Carlo process for the statistics of discrete systems*, *JETP Lett.*, 64 (1996), p. 911.
- [13] A. N. RUBTSOV, V. V. SAVKIN, AND A. I. LICHTENSTEIN, *Continuous-time quantum Monte Carlo method for fermions*, *Phys. Rev. B*, 72 (2005), p. 035122.
- [14] J. SCHACHENMAYER, A. PIKOVSKI, AND A. M. REY, *Many-body quantum spin dynamics with*



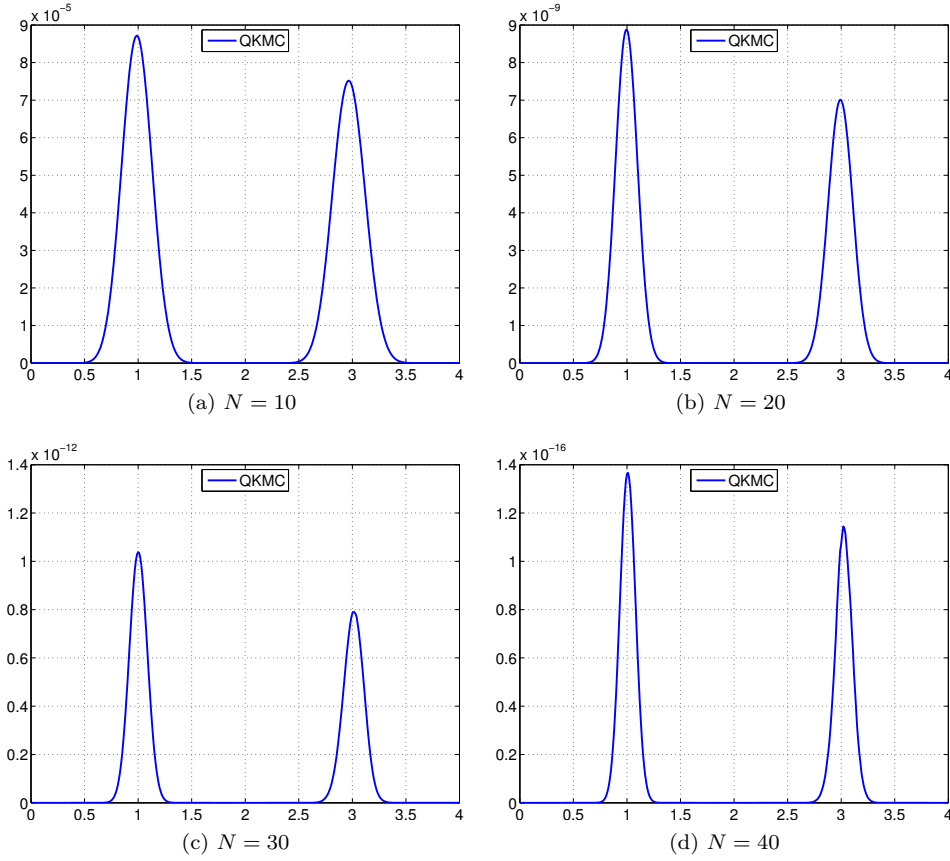


Fig. 4.7: Numerical tests with randomness,  $\gamma_0 = 0.01$

- monte carlo trajectories on a discrete phase space*, Phys. Rev. X, 5 (2015), p. 011022.
- [15] U. SCHOLLWÖCK, *The density-matrix renormalization group in the age of matrix product states*, Ann. Phys., 326 (2011), pp. 96–192.
- [16] R. L. STRATONOVICH, *On a method of calculating quantum distribution functions*, Soviet Physics Doklady, 2 (1958), p. 416.
- [17] G. VIDAL, *Efficient classical simulation of slightly entangled quantum computations*, Phys. Rev. Lett., 91 (2003), p. 147902.
- [18] S. R. WHITE, *Density matrix formulation for quantum renormalization groups*, Phys. Rev. Lett., 69 (1992), p. 2863.
- [19] S. ZHANG, *Auxiliary-field quantum Monte Carlo for correlated electron systems*, in Emergent Phenomena in Correlated Matter, Modeling and Simulation Vol. 3, Forschungszentrum Jülich, 2013.
- [20] S. ZHANG AND H. KRAKAUER, *Quantum Monte Carlo method using phase-free random walks with Slater determinants*, Phys. Rev. Lett., 90 (2003), p. 136401.